Research Article

Numerical Investigation of Wind Erosion to the Grooved Concrete Wall Surface under a Wind-Blown Sand Movement

Shanqun Chen [1,2] **Runchao Tang,** [1,2] **Longzhu Zhang,** [1,2] **and Bin Liao** [1,2]

[1]*College of Architecture and Civil Engineering, Anhui Polytechnic University, Anhui, Wuhu 241000, China*
[2]*Key Laboratory for Mechanics, Anhui Polytechnic University, Anhui, Wuhu 241000, China*

Correspondence should be addressed to Bin Liao; liaobinfluid@126.com

Wind erosion to the grooved concrete wall surface under a wind-blown sand movement was numerically studied. Particularly, the influencing factors that affect the wind erosion to the grooved concrete wall surface were systematically investigated by using the RNG $k - \varepsilon$ turbulence model combined with the discrete phase model (DPM). It was found that, under a relatively low impact angle, the damage mechanism to the grooved wall surface is wind-blown sand impact, and the erosion rates of the grooved wall surfaces are higher than those of the smooth wall surfaces. By contrast, under a relatively high impact angle, the damage mechanism to the grooved wall surface transfers to the microcutting effect, and the erosion rates show an opposite trend. The optimization rates between the erosion of grooved and smooth wall surfaces increase with increasing groove size or groove number. However, the damage mechanism to the grooved wall surface is hardly changed by expanding the groove area. The erosion rate distribution and the optimization rates of the groove wall surfaces are not significantly changed by adjusting the spacing between the grooves alone. When the groove shape changes from semicircular to rectangular, the erosion rate distribution is significantly changed, and the wear resistance of the changed grooved wall surface gets better.

1. Introduction

Wind erosion is usually caused by strong wind or sand particles carried by the wind, which is an inevitable problem in the long-term service of concrete structures. With the continued action of wind erosion, the concrete wall surface continues to peel off, the cracks expand and develop, the honeycomb surface deepens, and severe quality problems even occur, for instance, dew steel bars [1, 2]. Thus, wind erosion affects the aesthetics of the concrete structure and poses a threat to the service life and safety quality of it.

In practice, to aim at strengthening the concrete walls ability to resist wind erosion and reduce wind damage, the builders use methods such as increase mating ratios [3, 4] or overlay protective coatings [1, 5] to improve the wear resistance of concrete wall surface. However, these methods usually increase economic costs but do not achieve the desired results. Moreover, Momber [6, 7] found that the compressive strength, a traditional indicator parameter for

measuring concrete grades, was not an accurate assessment of wind erosion performance of concrete materials after comparing the performance of mortars, conventional concrete, and highly porous concrete specimens. Thus, there exist other factors that can strongly affect the wear resistance of concrete wall surface to wind erosion.

In the desert regions of nature, several living creatures have honed their skills to resist wind erosion during their long evolutionary evolution [8–10]. Moreover, to the cushioning effect of the superficial stratum corneum and subcutaneous soft tissue, these creatures usually have a unique body surface with complex texture structures, as shown in Figure 1. The improvement of texture structures to the wear resistance of wind erosion can be included in two aspects. Firstly, these texture structures can significantly alter the wind-sand flow around the body surface and the trajectories of sand particles carried by the wind. Secondly, these texture structures can strongly perturb the wind-sand

flow around the body surface and cause some changes in the area where wind erosion occurs.

Inspired by the texture structures of living creatures in the desert regions, there are many successful reducing applications of wear resistance, viscosity or drag in the aerospace, agricultural machinery, automotive industries, and so on. However, the related research in civil engineering field is relatively few. Particularly, the research of wind erosion to the concrete wall surface is rarely reported. Through the erosion experiments of concrete test blocks, Wang [11] and Hao [12] found that, with the erosion time increases, the smooth wall surface of the test block becomes uneven, the erosion rate tends to decrease instead, and wind erosion more likely occurs in the pits caused by the wind-blown sand impact. For nonsmooth concrete wall surface, Tang [13] studied the wind erosion to the grooved concrete wall surface which contains only one semicircular shape groove numerically. It was found that, compared to the smooth wall surface, the erosion rate of the grooved wall surface is different, and the erosion distribution on the grooved wall surface is obviously affected by the impact angle. However, this study is not sufficiently systematic, and further research is needed, such as specific parametric study and quantitative analysis.

In this paper, a numerical study that aims to reveal the influencing factors of wind erosion to the grooved concrete wall surface under a wind-blown sand movement is conducted using the RNG $k - \varepsilon$ turbulence model combined with the discrete phase model (DPM). The paper is organized as follows. First, the numerical model and validation are given. Then, we compare and analyze the numerical results between grooved and smooth concrete wall surfaces under different wind velocities and impact angles. The results under different groove sizes, groove numbers, and groove spacings are also presented and analyzed. Moreover, we change the groove shape to investigate the effect of erosion distribution on wind erosion. Finally, the main conclusions are drawn.

2. Numerical Model and Validation

2.1. Governing Equations.
The wind-blown sand movement is a typical wind-sand two-phase flow. Wind-sand two-phase flow is a flow system formed by the continuous phase (wind) and solid phase (sand particles). Correspondingly, the governing equations for wind-sand flow can be separately described by two aspects as follows.

2.1.1. Continuous Phase.
We selected the incompressible Reynolds Averaged Navier-Stokes (RANS) equations as the governing equations for continuous phase, which can be written as

$$\frac{\partial \overline{u}_i}{\partial x_i} = 0,$$

$$\frac{\partial \overline{u}_i}{\partial t} + \overline{u}_j \frac{\partial \overline{u}_i}{\partial x_j} = -\frac{1}{\rho}\frac{\partial \overline{p}}{\partial x_i} + \frac{\partial}{\partial x_j}\left[v\left(\frac{\partial \overline{u}_i}{\partial x_j} + \frac{\partial \overline{u}_j}{\partial x_i}\right) - \overline{u'_i u'_j} \right] + g,$$

(1)

where I and $j = 1$, 2, and 3 represent x, y, and z directions of Cartesian coordinates, respectively; g is the gravity; $\overline{u}_i$ is the averaged velocity over time; $\overline{u}'_i$ is the velocity fluctuation over time with $\overline{u'_i u'_j}$ representing the Reynolds stresses; ρ and v are the density and kinematic viscosity of the wind phase, respectively.

For wind erosion simulation scenarios, RANS turbulence modeling is very relevant, because of the spatial and temporal scales encountered in applications in wind engineering [14]. Here, we selected the renormalization group theory (RNG) $k - \varepsilon$ turbulence model, which uses a more effective viscosity to improve the performance of the model at low Reynolds numbers (Re) and considers the effect of swirl on turbulence near the wall surfaces [15]. The kinetic energy and dissipation rate of RNG $k - \varepsilon$ turbulence can be expressed as

$$\frac{\partial}{\partial t}(pk) + \frac{\partial}{\partial x_i}(pk\mu_i) = \frac{\partial}{\partial x_j}\left(\alpha_k \mu_{\text{eff}} \frac{\partial k}{\partial x_j}\right) + G_k + G_b - p\varepsilon,$$

$$\frac{\partial}{\partial t}(p\varepsilon) + \frac{\partial}{\partial x_i}(p\varepsilon\mu_i) = \frac{\partial}{\partial x_j}\left(\alpha_\varepsilon \mu_{\text{eff}} \frac{\partial \varepsilon}{\partial x_j}\right) + C_{1\varepsilon}G_k - C_{2\varepsilon}p\frac{\varepsilon^2}{k} - R_\varepsilon,$$

(2)

where G_k represents the generation of turbulence kinetic energy due to the mean velocity gradients; G_b is the generation of turbulence kinetic energy due to buoyancy; α_k and α_ε are the inverse effective Prandtl numbers for k and ε, respectively; they are set equal to 1.393; $C_{1\varepsilon}$ and $C_{2\varepsilon}$ are set equal to 1.42 and 1.68, respectively. The additional term R_ε is given by

$$R_\varepsilon = \frac{C_\mu \rho \eta^3 \left(1 - \eta/\eta_0\right)}{1 + \beta \eta^3}\frac{\varepsilon^2}{k},$$

(3)

where $\eta = Sk/\varepsilon$, $\eta_0 = 4.38$, and $\beta = 0.012$.

2.1.2. Solid Phase.
Here, we selected the DPM [16] that is based on the Euler-Lagrange method to obtain the trajectories of sand particles. Assuming that sand particles are relatively independent of each other and ignoring the effects of particle collisions and fragmentation, the force equilibrium equation for sand particle motion can be derived based on Newton's second law

$$\frac{d\overline{u}_p}{dt} = F_D\left(\overline{u}_c - \overline{u}_p\right) + \frac{g\left(\rho_p - \rho_c\right)}{\rho_p}, \tag{4}$$

where $\overline{u}_c$ and $\overline{u}_p$ are the averaged velocities of the continuous phase and sand particle, respectively; ρ_c and ρ_p are the densities of the continuous phase and sand particle, respectively; $F_D\left(\overline{u}_c - \overline{u}_p\right)$ is the unit mass drag force of sand particle; and F_D can be expressed as

$$F_D = \frac{18\mu_c}{\rho_p d_p^{\,2}} \frac{C_D\text{Re}}{24}, \tag{5}$$

where d_p is the diameter of the sand particle; μ_c is the viscosity of continuous phase; Re is the relative Reynolds number, $\text{Re} = \rho_c d_p |\overline{u}_p - \overline{u}_c|/\mu_c$; C_D is the drag coefficient, $C_D = 24/\text{Re}\left(1 + b_1\text{Re}^{b_2}\right) + b_3\text{Re}/b_4 + \text{Re}$; b_1, b_2, b_3, and b_4 are the shape coefficients of the sand particle.

2.2. Computational Domain. The schematic diagram of the computational domain is illustrated in Figure 2. To reduce the numerical errors, save the computational resources, and enhance the comparability of numerical results, we placed the grooved and smooth wall surfaces symmetrically in the same flow field. The width between the grooved and smooth wall surfaces is set about to 600 mm to avoid flow field interference between them. To meet the requirements of wind-sand flow development and exit obstruction rate, the front end of both wall surfaces is set equal to 200 mm from the inlet, and the rear end is set equal to 1000 mm from the outlet. Moreover, we adjusted the angles between the smooth or grooved wall surface and the wind-sand flow to achieve various impact angle conditions.

2.3. Numerical Conditions. We selected idea air as the continuous media of wind flow. Density and kinematic viscosity of it are 1.225 kg/m³ and 1.7894×10^{-5} kg/m·s, respectively. The mass flow of sand particles, carried by the wind flow, is 63 g/min. The diameter of the sand particle is 0.25 mm, the density of it is 2650 kg/m³, and the erosion time lasts for 3 min. The rebound recovery factor of the concrete wall surface to wind erosion is taken as 0.6. Considering the existence of critical velocities for wind erosion, we set the wind velocities at 19 m/s, 23 m/s, and 26 m/s to obtain noticeable wind erosion effects. Moreover, since there are differences in the damage mechanism of wind erosion on the concrete wall surface under different impact angles [17, 18], we finally selected the angles' range from 30° to 90° with a 15° interval, that is, 30°, 45°, 60°, 75°, and 90°, to systemically investigate the characteristics of wind erosion.

In addition, we selected a grooved and a smooth concrete wall surface as the simulation objects, where the smooth one is used to verify the reliability of the numerical model, and the grooved one is used to analyze the effects of influencing factors on the wear resistance of concrete wall surface to wind erosion. The material properties of the grooved and smooth concrete wall surfaces reference concrete test blocks which were used in the wind erosion experiment by Wang [11]. The raw materials of concrete test blocks include

cement (type P.O42.5), medium sand (fineness modulus = 2.83), crushed stone (particle size = 5–31.5 mm), and tap water. The sizes of the test blocks are 100 mm × 100 mm × 100 mm. The maintenance process of concrete test blocks is as follows. First, once the concrete test blocks were formed, they needed 24 hours to release the mold. Then, the test blocks were placed in a standard maintenance room (the temperature and relative humidity are set to (20 ± 2°C) and over 95%, resp.) for 28 days. Finally, the grade of concrete test blocks is C30, and their density is approximately 2400 kg/m³. Moreover, to avoid the effect of the flatness problems on the concrete wall surface, the roughness height of concrete test blocks is fixed to 2 mm.

2.4. Validation. It is necessary to note that wind erosion is usually stochastic; thus, local mass loss is challenging to predict accurately. However, the overall mass loss caused by wind erosion on the concrete wall surface of the same material is relatively stable, and the erosion rate over the erosion time can be used as a reliability validation of our numerical results. Through the steady-state particle tracking, the statistics of wind erosion on the wall surface can be obtained. Based on this, the calculation of erosion rate R_{erosion} can be expressed as

$$R_{\text{erosion}} = \sum_{p=1}^{N_{\text{particle}}} \frac{\dot{m}_p C\left(d_p\right) f\left(\alpha\right) v^{b(v)}}{A_{\text{face}}}, \tag{6}$$

where N_{particle} is the total number of sand particles; $\dot{m}_p$ is the mass flow of sand particles impacting the wall surface; $C\left(d_p\right)$ is a function of sand particle diameter; α is the impact angle of the particle path with the wall surface; $f\left(\alpha\right)$ is a function of the impact angle; v is the relative particle velocity; $b\left(v\right)$ is a function of relative particle velocity; and A_{face} is the area of the cell face at the wall surface.

The experimental results of wind erosion on 100 mm × 100 mm × 100 mm size test blocks [11], the numerical results in current work of the smooth wall surfaces at the same material and size, and the error rates between experimental and numerical results are shown in Figure 3. It is found that the numerical results of erosion amount increased significantly with increasing wind velocity and impact angle, which is consistent with Goretta [19] and Hao [20]. Moreover, the numerical results are generally close to those of the erosion experiments, with error rates basically from −4% to 6%, and the maximum error rate is 6.315%.

3. Results and Discussions

3.1. Effects of Wind Velocity and Impact Angle. The damage to concrete wall surfaces by sand particles is a direct source of wind erosion, and the kinetic energy of sand particles is mainly dependent on the ambient wind flow. In general, with increasing wind velocity, the sand particle gains more kinetic energy, causing more visible damage to the wall surface. To reveal the effects of wind velocity and impact angles on wind erosion and compare the wear resistance of grooved and smooth concrete wall surfaces, we obtained the

(a)   (b)

FIGURE 1: Local magnification of the body surfaces: (a) lizard; (b) diversiform-leaved poplar.
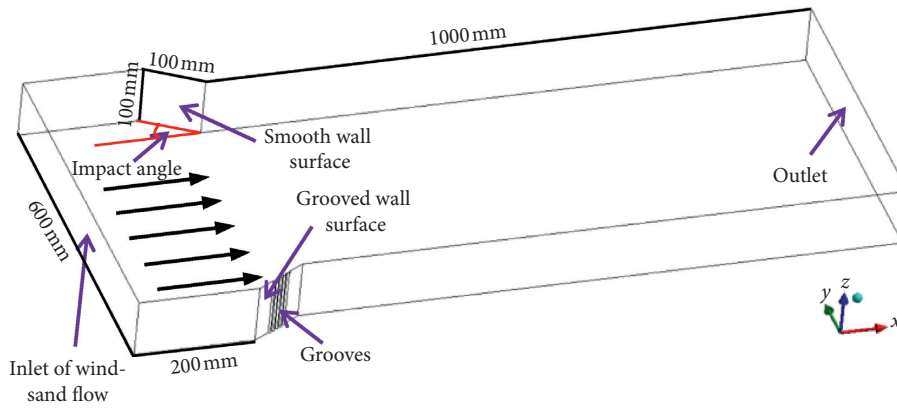

FIGURE 2: Schematic diagram of the computational domain. The black arrows indicate the sand particle path.

erosion rates of these wall surfaces under different wind velocities and impact angles, as listed in Table 1. It is necessary to note that there is only one semicircular shape groove located in the grooved wall surface, and the diameter of the groove is set equal to 6 mm. Considering that using larger velocities can save a lot of computing resources and highlight the effects of groove and impact angle to the wear resistance of wind erosion [21], the wind velocities of 19 m/s, 23 m/s, and 26 m/s are continuedly used in the next numerical calculations. The calculation of optimization rate is $e_{rs} - e_{rg}/e_{rs}$, where e_{rg} and e_{rs} are the erosion rates of grooved and smooth wall surfaces, respectively.

The erosion rates of the grooved wall surface significantly increase with increasing impact angle under different wind velocities, which is consistent with the results of the smooth wall surfaces. After being compared with the erosion rates of grooved and smooth wall surfaces at the same wind velocity and impact angle, it is found that the erosion rates of the grooved wall surfaces are higher than those of the smooth wall surfaces at the impact angles of 30° and 45°, while the erosion rates show an opposite trend at the impact angles of 60°, 75°, and 90°. With the increasing impact angle and wind velocity, the optimization rates between the erosion of grooved and smooth wall surfaces basically increase. However, under a relatively high impact angle (typically, 90°), the optimization rate is hardly affected by increasing wind velocity.

It is well accepted that concrete is a brittle material with high hardness and low toughness. The concrete wall surface contains defects such as floating slurry or microcracks, and the fragile parts containing these defects will wear away under wind erosion until the harder internal material is exposed. Thus, it is easier to wear the concrete wall surface by wind-blown sand impact, while it is relatively harder to wear it by microcutting effect [17, 18, 22, 23]. To comprehensively understand the mechanism of impact angle influence on the erosion rate, we obtained the typical trajectories of sand particles interaction with concrete wall surfaces at the impact angles of 30°, 60°, and 90° and the same wind velocity of 19 m/s, as shown in Figures 4–6. Here, we define the angles between the typical trajectory of inflow sand particles with the semicircular shape groove and smooth surfaces are α_i and β_i, respectively, where i represents the impact angle. It is found that $\alpha_{30°}$ is larger than $\beta_{30°}$, and the groove surface is subjected to more vertical impact than the smooth one. At the impact angle of 30°, compared to the smooth wall surface, the damage mechanism to the grooved wall surface by wind erosion is wind-blown sand impact. As listed in Table 1, the erosion rate of the grooved wall surface increases more than the smooth one with increasing wind velocity. Thus, the optimization rate increases with increasing wind velocity at the impact angle of 30°. At the impact angle of 60°, $\alpha_{60°}$ is close to $\beta_{60°}$, and the damage mechanism to the grooved wall surface is basically the same as the smooth one
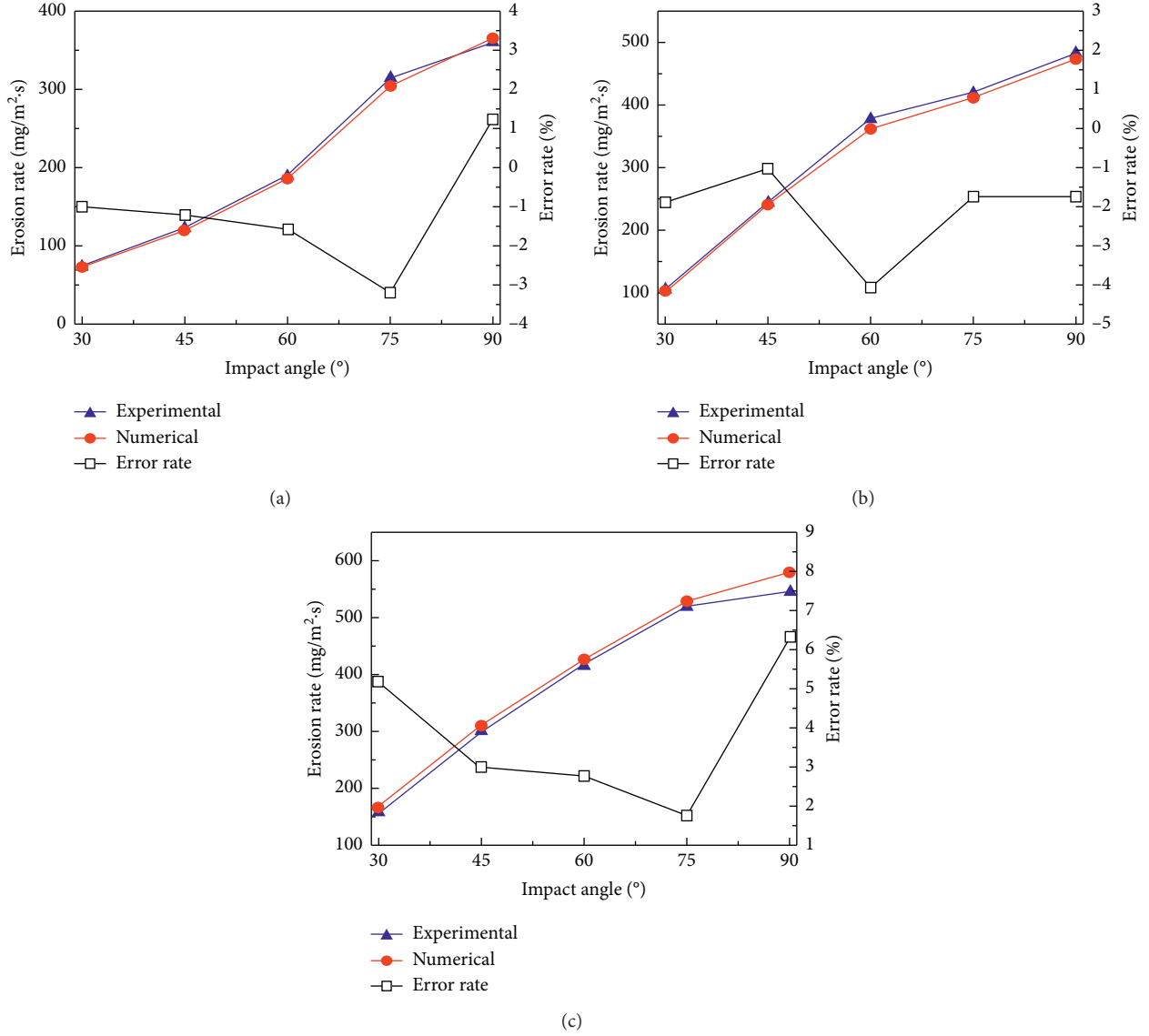
(a)

(b)

(c)

FIGURE 3: Experimental results, numerical results, and the error rates between them of wind erosion on smooth wall surfaces under different wind velocities: (a) 19 m/s; (b) 23 m/s; (c) 26 m/s.

TABLE 1: Erosion rates of grooved and smooth wall surfaces under different wind velocities and impact angles.

Impact angle (°)	Wind velocity (m/s)	Erosion rate of grooved wall surface e_{rg} (mg/m²·s)	Erosion rate of smooth wall surface e_{rs} (mg/m²·s)	Optimization rate (%)
30	19	$8.943E + 01$	$7.431E + 01$	−20.350
	23	$1.269E + 02$	$1.059E + 02$	−19.797
	26	$1.924E + 02$	$1.694E + 02$	−13.548
45	19	$1.282E + 02$	$1.214E + 02$	−5.552
	23	$2.449E + 02$	$2.387E + 02$	−2.614
	26	$3.211E + 02$	$3.159E + 02$	−1.653
60	19	$1.829E + 02$	$1.849E + 02$	1.109
	23	$3.580E + 02$	$3.685E + 02$	2.855
	26	$4.227E + 02$	$4.334E + 02$	2.471
75	19	$2.862E + 02$	$2.994E + 02$	4.397
	23	$3.961E + 02$	$4.121E + 02$	3.878
	26	$5.147E + 02$	$5.363E + 02$	4.026
90	19	$3.447E + 02$	$3.632E + 02$	5.084
	23	$4.638E + 02$	$4.876E + 02$	4.884
	26	$5.670E + 02$	$5.934E + 02$	4.457

Particle velocity magnitude

7.00e + 00   9.76e + 00   1.36e + 01   1.90e + 01
(m/s)

Typical trajectory of
outflow sand particles

Typical trajectory of
inflow sand particles

Grooved wall surface $\alpha_{30°}$

Semicircular shape groove

(a)

Particle velocity magnitude

9.00e + 00   1.15e + 01   1.48e + 01   1.90e + 01
(m/s)

Typical trajectory of
outflow sand particles

Typical trajectory of
inflow sand particles

$\beta_{30°}$

Smooth wall surface

(b)
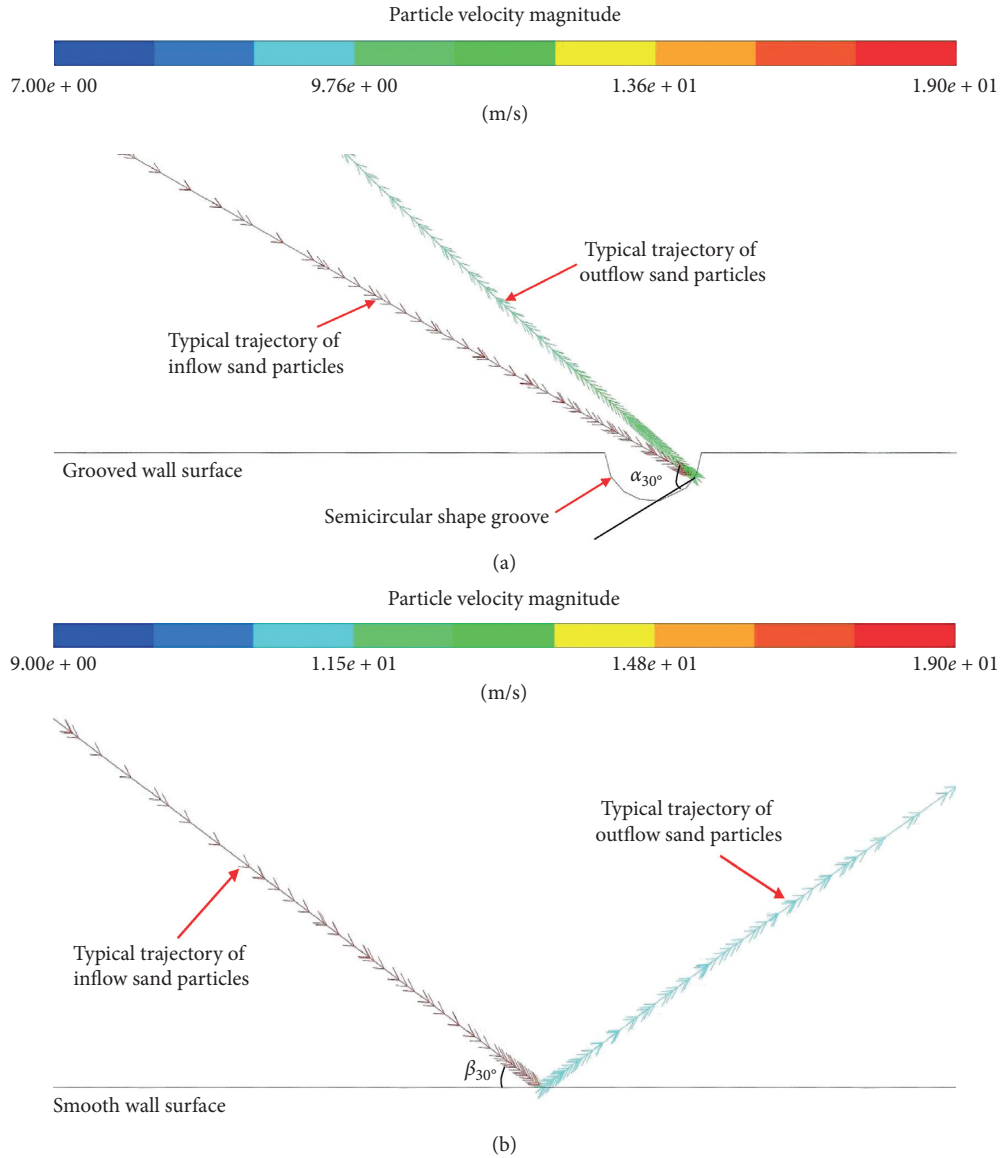
FIGURE 4: Typical trajectories of sand particles interaction with concrete wall surfaces at the impact angle of 30° and wind velocity of 19 m/s: (a) grooved; (b) smooth.

by wind erosion. The optimization rate between the grooved and smooth wall surfaces is close to zero. At the impact angle of 90°, $\alpha_{90°}$ is smaller than $\beta_{90°}$, and the damage mechanism to the grooved wall surface by wind erosion transfers to the microcutting effect. Thus, the optimization rate is hardly affected by increasing wind velocity due to the high strength properties of concrete interior materials at the impact angle of 90°. These results clearly reveal the mechanism of impact angle and wind velocity influence on the erosion rates.

3.2. Effects of Groove Size and Groove Number. When the groove area is small, the effect of the groove on wind erosion to the grooved wall surface is less pronounced. By expanding the groove area, we can further reveal the mechanism of expanding groove influence on wind erosion. Here, we

achieved the expansion of the groove area by enlarging the diameter of the semicircular shape groove or increasing the number of grooves.

Table 2 lists the erosion rates of grooved and smooth wall surfaces under the groove sizes of 6 mm, 12 mm, and 18 mm and the same wind velocity of 19 m/s. It is found that the erosion rates of the grooved wall surfaces are higher than those of the smooth wall surfaces at the impact angles of 30° and 45°, while the erosion rates show an opposite trend at the impact angles of 60°, 75°, and 90°. These results are similar to those in Table 1. Moreover, under a relatively low impact angle (typically, 30° and 45°), the negative optimization rates between the erosion of grooved and smooth wall surfaces increase with increasing groove size. By contrast, under a relatively high impact angle (typically, 75° and 90°), the positive optimization rate shows the same trend with
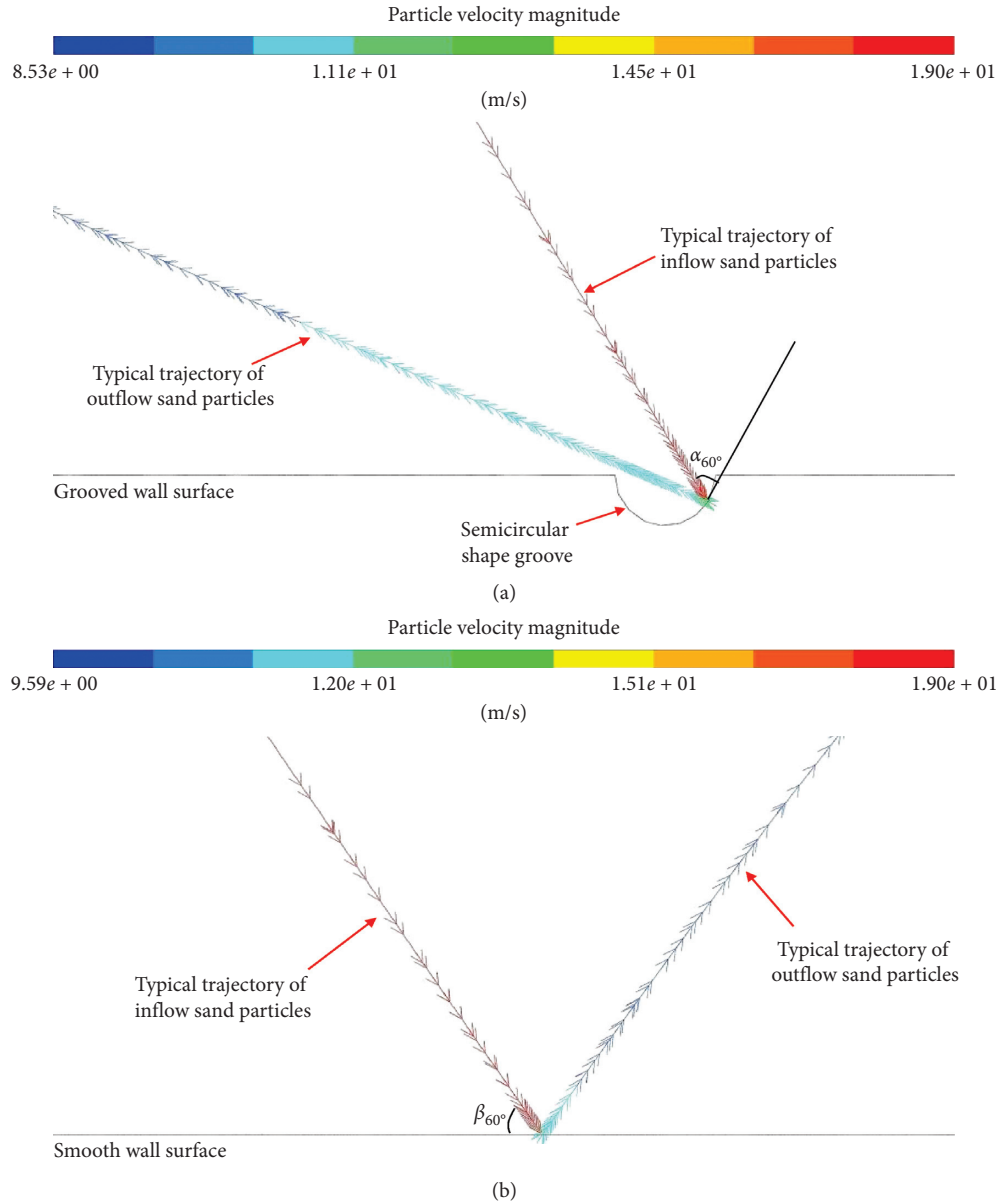
FIGURE 5: Typical trajectories of sand particles interaction with concrete wall surfaces at the impact angle of 60° and wind velocity of 19 m/s: (a) grooved; (b) smooth.

increasing groove size. Thus, the applicable impact angle of the grooved wall surface is still 60° or more.

Table 3 lists the erosion rates of grooved and smooth wall surfaces under the groove numbers of 1, 3, and 5 and the same wind velocity of 19 m/s. It is necessary to note that the groove size is set equal to 6 mm. It is found that the erosion rates of the grooved wall surfaces are higher than those of the smooth wall surfaces at the impact angles of 30° and 45°, while the erosion rates show an opposite trend at the impact angles of 60°, 75°, and 90°. These results are still similar to those in Table 1 and Table 2. Moreover, under a relatively low impact angle (typically, 30° and 45°), the negative optimization rates between the erosion of grooved and smooth wall surfaces increase with increasing groove number. By contrast, under a relatively high impact angle (typically, 75° and 90°), the positive optimization rate shows

Particle velocity magnitude

8.00e + 00   1.07e + 01   1.42e + 01   1.90e + 01

(m/s)

Typical trajectory of
inflow sand particles

Typical trajectory of
outflow sand particles

$\alpha_{90°}$

Grooved wall surface

Semicircular
shape groove

(a)

Particle velocity magnitude

7.00e + 00   9.76e + 01   1.36e + 01   1.90e + 01

(m/s)

Typical trajectory of
outflow sand particles

Typical trajectory of
inflow sand particles
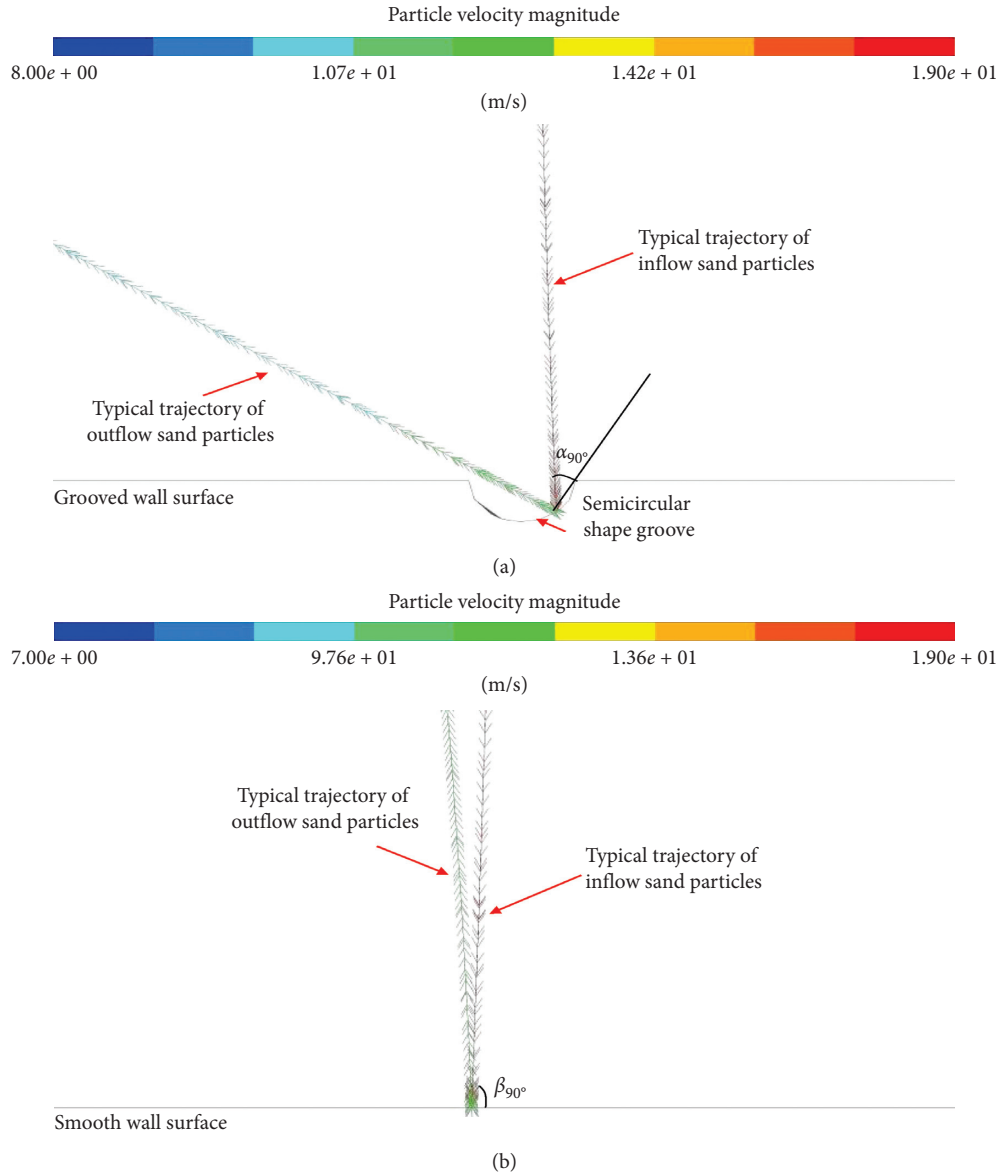
$\beta_{90°}$

Smooth wall surface

(b)

Figure 6: Typical trajectories of sand particles interaction with concrete wall surfaces at the impact angle of 90° and wind velocity of 19 m/s: (a) grooved; (b) smooth.

the same trend with increasing groove number. These results clearly reveal that the effect of impact angle on wind erosion is almost unchanged by expanding the groove area, but the negative or positive optimization rates of wind erosion both increase by it.

3.3. Effect of Groove Spacing. The groove distribution is another influencing factor of wind erosion. By changing the area where the groove locates, we can investigate the effect of groove distribution on wind erosion to the grooved wall surface. Here, we achieved the changing of the groove distribution by adjusting the spacing between the grooves.

Table 4 lists the erosion rates of grooved and smooth wall surfaces under the groove spacings of 2 mm, 4 mm, and 6 mm and the same wind velocity of 19 m/s. It is necessary to note that the groove size is set equal to 6 mm, and the groove

TABLE 2: Erosion rates of grooved and smooth wall surfaces under different groove sizes and impact angles.

Impact angle (°)	Groove size (mm)	Erosion rate of grooved wall surface e_{rg} (mg/m²·s)	Erosion rate of smooth wall surface e_{rs} (mg/m²·s)	Optimization rate (%)
30	6	$8.943E + 01$	$7.431E + 01$	−20.350
	12	$9.803E + 01$	$7.429E + 01$	−31.960
	18	$1.107E + 02$	$7.420E + 01$	−49.237
45	6	$1.282E + 02$	$1.214E + 02$	−5.552
	12	$1.341E + 02$	$1.214E + 02$	−10.392
	18	$1.384E + 02$	$1.215E + 02$	−13.912
60	6	$1.829E + 02$	$1.849E + 02$	1.109
	12	$1.814E + 02$	$1.848E + 02$	1.832
	18	$1.799E + 02$	$1.849E + 02$	2.664
75	6	$2.862E + 02$	$2.994E + 02$	4.397
	12	$2.744E + 02$	$2.993E + 02$	8.317
	18	$2.610E + 02$	$2.991E + 02$	12.733
90	6	$3.447E + 02$	$3.632E + 02$	5.084
	12	$3.250E + 02$	$3.632E + 02$	10.516
	18	$3.089E + 02$	$3.631E + 02$	14.914

TABLE 3: Erosion rates of grooved and smooth wall surfaces under different groove numbers and impact angles.

Impact angle (°)	Groove number	Erosion rate of grooved wall surface e_{rg} (mg/m²·s)	Erosion rate of smooth wall surface e_{rs} (mg/m²·s)	Optimization rate (%)
30	1	$8.943E + 01$	$7.431E + 01$	−20.347
	3	$1.120E + 02$	$7.418E + 01$	−50.984
	5	$1.357E + 02$	$7.424E + 01$	−82.786
45	1	$1.282E + 02$	$1.214E + 02$	−5.601
	3	$1.400E + 02$	$1.218E + 02$	−14.943
	5	$1.494E + 02$	$1.217E + 02$	−22.761
60	1	$1.829E + 02$	$1.849E + 02$	1.082
	3	$1.802E + 02$	$1.850E + 02$	2.595
	5	$1.773E + 02$	$1.847E + 02$	4.006
75	1	$2.862E + 02$	$2.994E + 02$	4.409
	3	$2.629E + 02$	$2.993E + 02$	12.162
	5	$2.432E + 02$	$2.995E + 02$	18.798
90	1	$3.447E + 02$	$3.632E + 02$	5.094
	3	$3.098E + 02$	$3.627E + 02$	14.585
	5	$2.799E + 02$	$3.629E + 02$	22.871

TABLE 4: Erosion rates of grooved and smooth wall surfaces under different groove spacings and impact angles.

Impact angle (°)	Groove spacing (mm)	Erosion rate of grooved wall surface e_{rg} (mg/m²·s)	Erosion rate of smooth wall surface e_{rs} (mg/m²·s)	Optimization rate (%)
30	2	$1.357E + 02$	$7.424E + 01$	−82.786
	4	$1.344E + 02$	$7.436E + 01$	−80.742
	6	$1.331E + 02$	$7.434E + 01$	−79.042
45	2	$1.494E + 02$	$1.217E + 02$	−22.761
	4	$1.490E + 02$	$1.216E + 02$	−22.533
	6	$1.471E + 02$	$1.216E + 02$	−20.970
60	2	$1.773E + 02$	$1.847E + 02$	4.006
	4	$1.766E + 02$	$1.848E + 02$	4.437
	6	$1.778E + 02$	$1.847E + 02$	3.736
75	2	$2.432E + 02$	$2.995E + 02$	18.798
	4	$2.409E + 02$	$2.993E + 02$	19.512
	6	$2.409E + 02$	$2.991E + 02$	19.458
90	2	$2.799E + 02$	$3.629E + 02$	22.871
	4	$2.799E + 02$	$3.630E + 02$	22.893
	6	$2.804E + 02$	$3.629E + 02$	22.734

number is set equal to 5. It is found that the erosion rates of the grooved wall surfaces are higher than those of the smooth wall surfaces at the impact angles of 30° and 45°, while the erosion rates show an opposite trend at the impact angles of 60°, 75°, and 90°. These results are still similar to those in Tables 1–3, and the effect of impact angle on wind erosion to the grooved wall surface is almost unaffected by increasing groove spacing. Moreover, different from the results listed in Tables 2 and 3, under all impact angles, the negative or positive optimization rates between the erosion of grooved and smooth wall surfaces hardly change with increasing groove spacing. To reveal the reasons for these results, Figure 7 shows wind erosion rate distribution on the grooved wall surfaces at the impact angle of 90° and wind velocity of 19 m/s under groove spacings of 2 mm, 4 mm, and 6 mm, respectively. It is found that the erosion rate distribution is relatively similar between Figure 7(a)–7(c). Combined with the results in Table 4 and Figure 7, we can find that adjusting the spacing between the grooves alone without other measures does not significantly change the erosion rate distribution and the optimization rates of the groove wall surfaces.

3.4. Effect of Groove Shape.

3.4. Effect of Groove Shape. In general, the erosion rate distribution is a critical influencing factor of wind erosion. However, from the previous section, we found that the erosion rate distribution is not significantly changed without changing the groove shape. Thus, in this section, we expect to change the erosion rate distribution and achieve a higher optimization rate by changing the groove shape.

Here, to aim at a similar area with the semicircular shape groove, we selected the rectangular shape groove as the subject for research. Figure 8 shows the diagram of the groove changes from the semicircular shape to the rectangular shape. To reveal the effect of groove shape on wind erosion and compare the wear resistance of changed grooved and smooth concrete wall surfaces, we obtained the erosion rates of these wall surfaces under different wind velocities and impact angles, as listed in Table 5. It is necessary to note that there is only one rectangular shape groove located in the changed grooved wall surface. It is found that the erosion rates of the changed grooved wall surfaces are higher than those of the smooth wall surfaces at the impact angles of 30°, while the erosion rates show an opposite trend at the impact angles of 45°, 60°, 75°, and 90°. Moreover, under impact angles of 45°, 60°, 75°, and 90°, the optimization rate is hardly affected by increasing wind velocity.

Comparing the results listed in Tables 1 and 5, there are two main differences between them. Firstly, the positive optimization rate appears when the impact angle is larger than 45° in Table 5, while the impact angle needs to be larger than 60° in Table 1. Secondly, the optimization rate is always larger in Table 5; that is, the wear resistance of the grooved wall surface which contains a rectangular shape groove is

TABLE 5: Erosion rates of changed grooved and smooth wall surfaces under different wind velocities and impact angles.

Impact angle (°)	Wind velocity (m/s)	Erosion rate of changed grooved wall surface e_{rg} (mg/m²·s)	Erosion rate of smooth wall surface e_{rs} (mg/m²·s)	Optimization rate (%)
30	19	$8.035E + 01$	$7.435E + 01$	−8.070
	23	$1.204E + 02$	$1.057E + 02$	−13.907
	26	$1.824E + 02$	$1.689E + 02$	−7.993
45	19	$1.181E + 02$	$1.214E + 02$	2.718
	23	$2.324E + 02$	$2.388E + 02$	2.680
	26	$3.070E + 02$	$3.158E + 02$	2.787
60	19	$1.741E + 02$	$1.843E + 02$	5.534
	23	$3.466E + 02$	$3.680E + 02$	5.815
	26	$4.088E + 02$	$4.331E + 02$	5.611
75	19	$2.818E + 02$	$2.998E + 02$	6.004
	23	$3.884E + 02$	$4.133E + 02$	6.025
	26	$5.061E + 02$	$5.384E + 02$	5.999
90	19	$3.422E + 02$	$3.631E + 02$	5.756
	23	$4.588E + 02$	$4.868E + 02$	5.752
	26	$5.583E + 02$	$5.922E + 02$	5.724

basically better than the one that contains a semicircular shape groove.

To reveal the reasons for the differences, we obtained the typical trajectories of sand particles interaction with the two different grooved concrete wall surfaces at the impact angle of 45° and wind velocity of 23 m/s, as shown in Figure 9. It is found that the typical trajectory of inflow sand particles in Figure 9(a) only experiences one bounce, and the velocity of sand particles does not drop significantly. By contrast, in Figure 9(b), the typical trajectory of inflow sand particles experiences two bounces, and the velocity of sand particles drops significantly. Thus, on the one hand, the reduction of velocity leads to a reduction in the kinetic energy of sand particles that impact the wall surface. On the other hand, due to the two bounces of sand particles and the blocking effect of the sidewall, the leeward sidewall surface in Figure 9(b) is hard to subject the impact by the sand particles. Thus, compared to the results listed in Table 1, the erosion rate of the changed grooved wall surface decreases. Moreover, to reveal the effect of groove shape on wind erosion distribution, we obtained wind erosion rate distribution on the two different grooved wall surfaces at the impact angle of 45° and wind velocity of 23 m/s, as shown in Figure 10. It is found that the erosion rate distribution is different between the two grooved wall surfaces. As illustrated in Figure 10(a), uneven wind erosion is distributed on the area in front of the groove and on the area behind the groove. By contrast, wind erosion is relatively evenly distributed on the area in front of the groove and on the area behind the groove in Figure 10(b). Compared to the erosion rate in Figure 10(a), the erosion rate (especially the erosion rate of the groove

DPM erosion rate (generic)

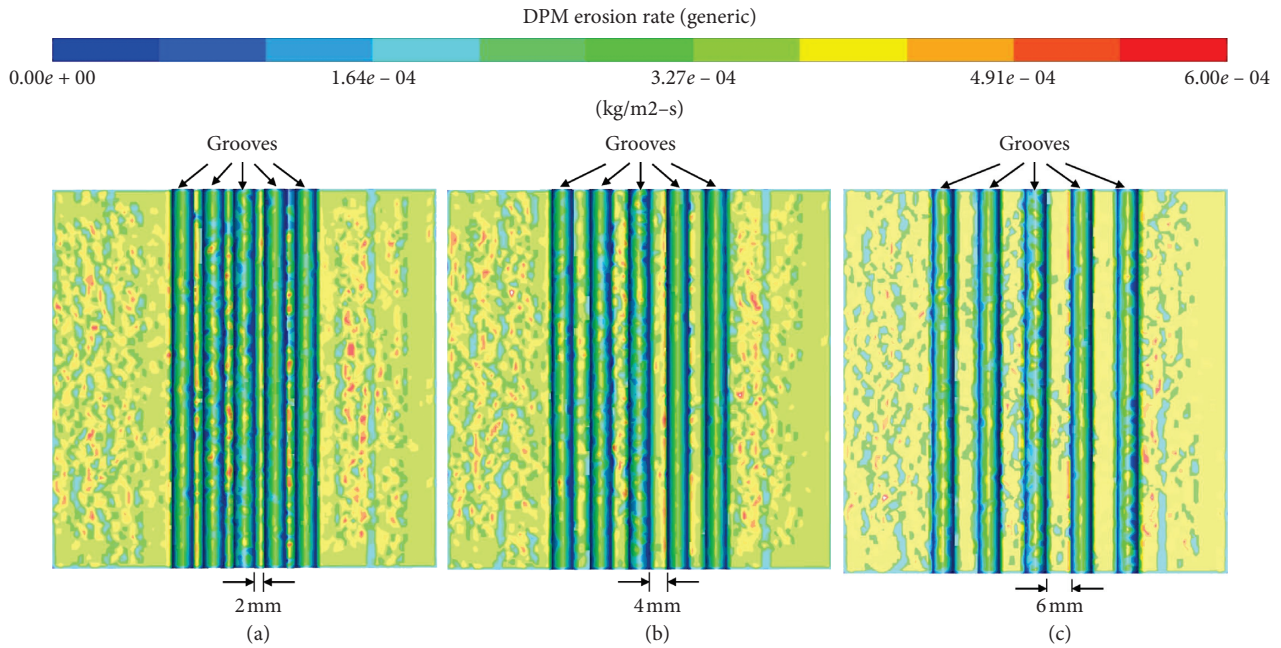| 0.00e + 00 | 1.64e − 04 | 3.27e − 04 | 4.91e − 04 | 6.00e − 04 |

(kg/m2–s)

FIGURE 7: Wind erosion rate distribution on the grooved wall surfaces at the impact angle of 90° and wind velocity of 19 m/s under different groove spacings: (a) 2 mm; (b) 4 mm; (c) 6 mm.
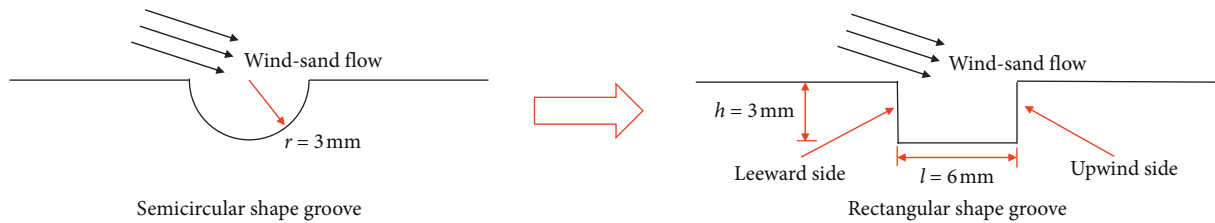

FIGURE 8: Schematic diagram of the groove changes from the semicircular shape to the rectangular shape. (r), (h), and (l) represent the radius of the semicircular shape groove, the height of the rectangular shape groove, and the length of the bottom side of the rectangular shape groove, respectively.

Particle velocity magnitude

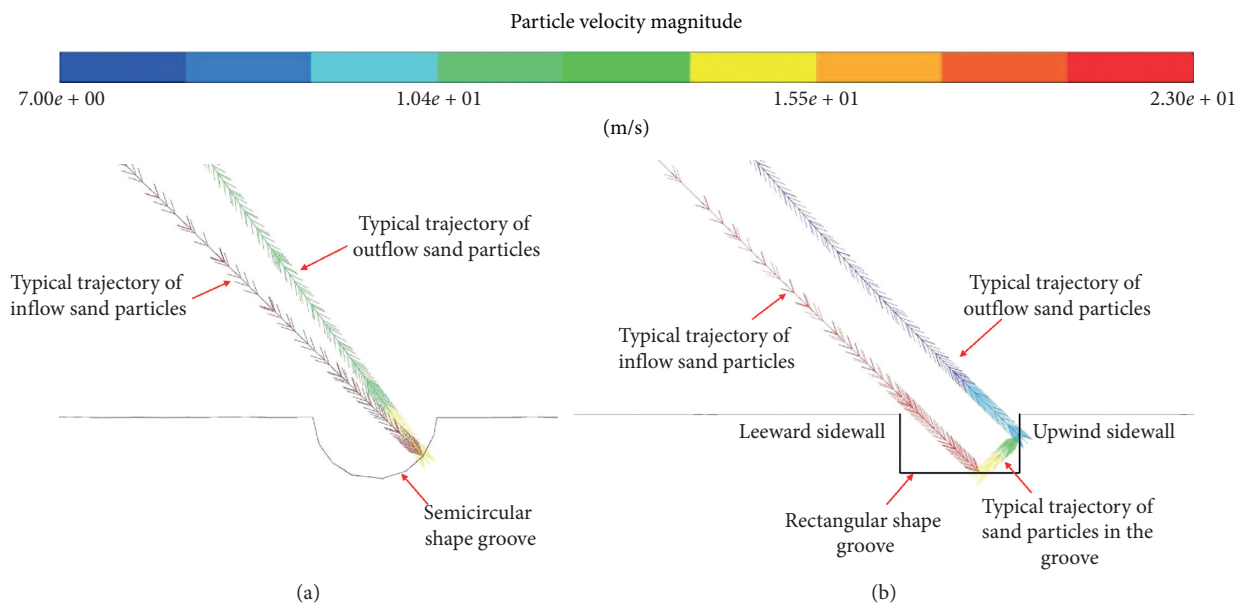| 7.00e + 00 | 1.04e + 01 | 1.55e + 01 | 2.30e + 01 |

(m/s)

FIGURE 9: Typical trajectories of sand particles interaction with two different grooved concrete wall surfaces at the impact angle of 45° and wind velocity of 23 m/s: (a) semicircular shape groove; (b) rectangular shape groove.
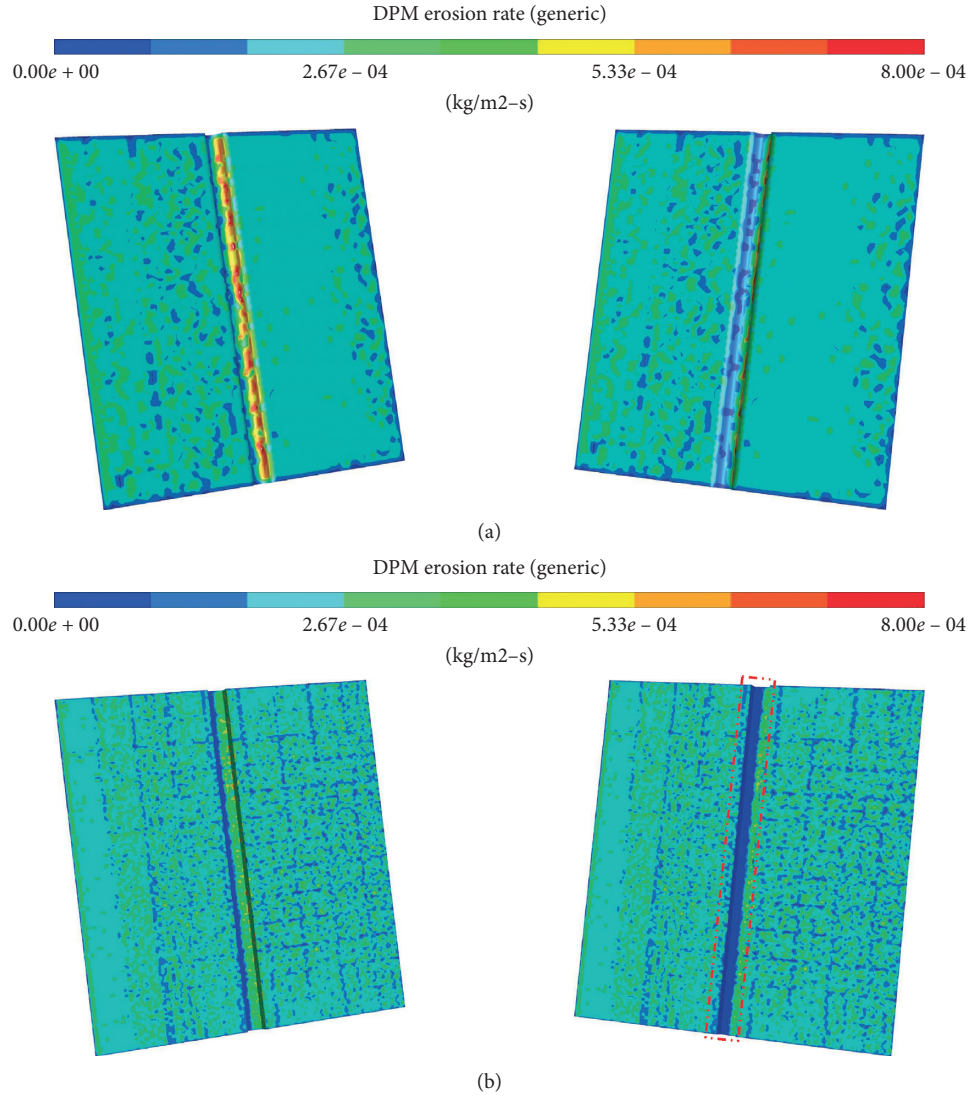
DPM erosion rate (generic)

(a)

DPM erosion rate (generic)

(b)

FIGURE 10: Wind erosion rate distribution on the two different grooved wall surfaces at the impact angle of 45° and wind velocity of 23 m/s: (a) side views of erosion rate distribution on the grooved wall surface which contains a semicircular shape groove; (b) side views of erosion rate distribution on the grooved wall surface which contains a rectangular shape groove.

area) is smaller in Figure 10(b). Moreover, the red-dotted line box in Figure 10(b) clearly shows that about half of the groove area hardly is subject to wind erosion due to the blocking effect of the sidewall.

4. Conclusions

Wind erosion to the grooved concrete wall surface under a wind-blown sand movement was studied using a numerical method. The wind-sand two-phase flow of wind erosion was solved by the RNG $k - \varepsilon$ turbulence model combined with the DPM. The numerical results between grooved and smooth concrete wall surfaces under different wind velocities and impact angles were compared to reveal the effects of wind velocity and impact angle on wind erosion. In addition, other influencing factors for wind erosion, such as groove

size, groove number, groove spacing, and groove shape, were also studied. The following conclusions can be drawn:

(1) Under a relatively low impact angle (typically, 30° and 45°), compared to the smooth wall surface, the damage mechanism to the grooved wall surface is wind-blown sand impact, and the erosion rates of the grooved wall surfaces are higher than those of the smooth wall surfaces. By contrast, under a relatively high impact angle (typically, 75° and 90°), the damage mechanism to the grooved wall surface transfers to the microcutting effect, and the erosion rates show an opposite trend.

(2) The negative or positive optimization rates between the erosion of grooved and smooth wall surfaces increase with increasing groove size or groove number. However, the effect of impact angle on the

wind erosion is unchanged, and the applicable impact angle of the grooved wall surface is still 60° or more.

(3) Adjusting the spacing between the grooves alone without other measures does not significantly change the erosion rate distribution and the optimization rates of the groove wall surfaces.

(4) When the groove shape changes from semicircular to rectangular, the erosion rate distribution is significantly changed, and the wear resistance of the changed grooved wall surface is basically better than the original one. Moreover, the applicable impact angle of the changed grooved wall surface drops from 60° to 45°.

Data Availability

The data that support the findings of this study are available from the corresponding author (Bin Liao) upon reasonable request.

Conflicts of Interest

The authors declare that they have no conflicts of interest.

Acknowledgments

References

[1] Y. P. Wang, Q. C. Wang, and C. C. Ju, "Effect of concrete surface treatment on anti-erosion performance (in Chinese)," *Concrete*, vol. 3, pp. 37–40, 2013.

[2] Y. P. Wang, Z. Gong, and Q. C. Wang, "Solid-particle erosion of concrete bridge piers and protective material under blown sand environment (in Chinese)," *Bulletin of the Chinese Ceramic Society*, vol. 34, no. 7, pp. 1941–1946, 2015.

[3] H. F. Li and Y. Xia, "Influence of limestone powder and carbon fiber on wear resistance of super-high strength high performance concrete (in Chinese)," *Bulletin of The Chinese Ceramic Society*, vol. 32, no. 4, pp. 635–639, 2013.

[4] H. Li, D. Y. Yang, W. Shen et al., "Effect of nickel slag to wear resistance of concrete (in Chinese)," *Bulletin of the Chinese Ceramic Society*, vol. 34, no. 11, pp. 3122–3128, 2015.

[5] Y. P. Wang, Z. Gong, and Q. C. Wang, "Solid particle erosive wear of epoxy and its composites (in Chinese)," *Journal of Building Materials*, vol. 18, no. 4, pp. 652–657, 2015.

[6] A. W. Momber, "The erosion of cement paste, mortar and concrete by gritblasting," *Wear*, vol. 246, no. 1-2, pp. 46–54, 2000.

[7] A. W. Momber, "Damage to rocks and cementitious materials from solid impact," *Rock Mechanics and Rock Engineering*, vol. 37, no. 1, pp. 57–82, 2004.

[8] Y. X. Lu, "Significance and progress of bionics," *Journal of Bionics Engineering*, vol. 1, no. 1, pp. 1–3, 2004.

[9] W. Baumgartner, F. Saxe, A. Weth et al., "The sandfish′s skin: morphology, chemistry and reconstruction," *Journal of Bionic Engineering*, vol. 4, no. 1, pp. 1–9, 2007.

[10] X. P. Hajas, "Mechanism analysis of anti-erosion wear based on the bionic pit form of desert Lizard′s skin (in Chinese)," *Journal of Beijing University of Technology*, vol. 41, no. 07, pp. 980–983, 2015.

[11] Y. P. Wang, C. C. Ju, and Q. C. Wang, "Influence of impact parameters on the erosion wear of Lanxin railway concrete structure (in Chinese)," *Bulletin of The Chinese Ceramic Society*, vol. 32, no. 4, pp. 607–612, 2013.

[12] Y. H. Hao, Y. L. Liu, J. C. Fan et al., "Research on erosion property of concrete and carbonation depth under gas-solid two-phase flow (in Chinese)," *Concrete*, vol. 6, pp. 27–30, 2016.

[13] R. C. Tang, S. Q. Chen, B. Liao et al., "Research on the anti-wind erosion of concrete wall with single groove shape (in Chinese)," *Journal of Anhui Polytechnic University*, vol. 34, no. 1, pp. 59–64, 2019.

[14] J. Franke, C. Hirsch, G. Jensen et al., "Recommendations on the use of CFD in wind engineering," in *Proceedings of the International Conference on Urban Wind Engineering and Building Aerodynamics*, pp. C.1.1–C1.11, Belgium, Europe, October 2004.

[15] G. Alfonsi, "Reynolds-averaged Navier–Stokes equations for turbulence modeling," *Applied Mechanics Reviews*, vol. 62, no. 4, Article ID 040802, 2009.

[16] N. M. Zahari, M. H. Zawawi, L. M. Sidek et al., "Introduction of discrete phase model (DPM) in fluid flow: a review," *AIP Conference Proceedings*, vol. 2030, no. 1, Article ID 020234, 2018.

[17] I. Finnie, "Erosion of surfaces by solid particles," *Wear*, vol. 3, no. 2, pp. 87–103, 1960.

[18] G. L. Sheldon and A. Kanhere, "An investigation of impingement erosion using single particles," *Wear*, vol. 21, no. 1, pp. 195–209, 1972.

[19] K. C. Goretta, M. L. Burdt, M. M. Cuber et al., "-particle erosion of Portland cement and concrete," *Wear*, vol. 224, no. 1, pp. 106–112, 1999.

[20] Y. Perry, Y. Feng, and J. Fan, "Experimental study into erosion damage mechanism of concrete materials in a wind-blown sand environment," *Construction and Building Materials*, vol. 111, pp. 662–670, 2016.

[21] Y. P. Wang, C. C. Ju, and Q. C. Wang, "Experimental study on the solid particle erosion of concrete, mortar and cement paste under blown sand environment (in Chinese)," *China Railway Science*, vol. 34, no. 5, pp. 21–26, 2013.

[22] G. L. Sheldon and I. Finnie, "On the ductile behavior of nominally brittle materials during erosive cutting," *Journal of Engineering for Industry*, vol. 88, no. 4, pp. 387–392, 1966.

[23] A. G. Evans and T. R. Wilshaw, "Quasi-static solid particle damage in brittle solids-I. Observations analysis and implications," *Acta Metallurgica*, vol. 24, no. 10, pp. 939–956, 1976.